Solution of the $1T_2$ discommensurate state of 1T-TaS_2. An example of rotated hexagonal discommensuration

1990 J. Phys.: Condens. Matter 2 1683

(http://iopscience.iop.org/0953-8984/2/7/002)

J. Phys.: Condens. Matter **2** (1990) 1683–1704. Printed in the UK

Solution to the $1T_2$ discommensurate state of 1T-TaS_2. An example of rotated hexagonal discommensuration

John A Wilson
H H Wills Physics Laboratory, University of Bristol, Bristol BS8 1TL, UK

Received 11 August 1989

Abstract. The discommensurate structure of $1T_2$-TaS_2 has been resolved by combining electron diffraction results with very recent scanning tunnelling microscopy data. The solution is provided by the hitherto unconsidered $19\frac{2}{3}$-by-$2\frac{2}{3}$ rotated honeycomb array of discommensurations (DCs). Being non-integral but rational, these numbers relate to a yet larger supercell for the $1T_2$ state, giving an associated ultra-fine micro-mesh in reciprocal space upon which to base the diffraction pattern. The resulting enlarged and 30° rotated cell is well suited to an ABC three-sandwich stacking sequence for the honeycomb arrays, without any further cell enlargement. Within each individual sandwich the DC honeycombs themselves are just over 70 Å across, very much as for the hitherto considered 18-by-5 rotated, discommensurate superstate. The actual DC phase-jog is precisely as for 18-by-5, but only one in three of the DC domains find themselves centred by a CDW thirteen-atom star. The final $1T_2$ structure succeeds in not stacking its CDW charge hills (and their concomitant distortions) directly above each other. The favoured ABC domain stack, however, impairs DC array visibility. Some discussion is finally given regarding further possible states on the approach to full $\sqrt{13}a_0$ commensuration.

1. Introduction

Scanning tunnelling microscopy has recently provided direct confirmation of the long-inferred discommensurate character of the $1T_2$ phase of 1T-TaS_2 [1]. The $1T_2$ phase is the 'quasi-commensurate' CDW phase [2] found between 352 K and 180 K on cooling (or 270 K and 352 K on warming). It is the intermediate CDW phase between $1T_1$, the axially aligned, high temperature, incommensurate phase (where $\boldsymbol{q}_I = 0.288\,\boldsymbol{a}_0^* \simeq \frac{2}{7}\boldsymbol{a}_0^*$)†, and $1T_3$, the rotationally locked-in $\sqrt{13}\,a_0^*$ phase. The latter involves a 3-by-1 basal plane rotation of 13°54′, with $|\boldsymbol{q}_I| = (1/\sqrt{13})a_0^* = 0.2773\,a_0^*$. The CDW/PLD amplitude in all three states is large (≃0.3 Å) [3–5] and given our experience in the 2H-TaS_2 family of materials [6–8], where the amplitude is only ≃0.1 Å or less, it has been anticipated that the $1T_1$ and $1T_2$ phases should both prove to be strongly discommensurate. For the 2H materials the discommensuration (DC) arrays were discovered as very evident features in dark-field electron microscopy [6]. The arrays were observed to be significantly disordered due to local pinning. The effective ICDW wavevector seems in 2H to shift with temperature in a smooth though non-monotonic fashion from an onset value of $0.324\,\boldsymbol{a}_0^*$ towards a lock-in at $\boldsymbol{a}_0^*/3$ [9]. As the DCs become more widely spaced in this process, so the array becomes more disordered by local pinning. Close to lock-in it

† Throughout we quote only the basal plane component to such wavevectors.

0953-8984/90/071683 + 22 $03.50

becomes possible to observe just why the discommensurate behaviour of the 2H material is so visible under dark-field EM imaging. The dominant contrast in the image in fact is areal contrast from the effectively commensurate regions between the DCs, and is not line contrast from the phase-slip regions of the DCs themselves. The origin of the dark-field areal contrast is the adoption of a phasing for the commensurate $3a_0$ CDW that actually breaks hexagonal symmetry slightly. The reduced symmetry is orthorhombic. With this, the DC array of the 2H ICDW state becomes not a simple honeycomb (as earlier theory had anticipated [10]) but a double honeycomb defining diamond-shaped domains of twin-like interrelation [6].

For the $1T_2$ and $1T_1$ states much effort has gone into trying to image DC arrays in a variety of ways, but always without success [11]. This has been especially disappointing for the $1T_2$ state since the latter displays a very characteristic complex diffraction pattern, much as for a shear structure. Indeed the pattern led us originally to call the $1T_2$ state 'quasi-commensurate' [2] prior to the more general notion of 'discommensurate' being developed [10]. Part of the reason for the lack of any easy success is the matter of symmetry outlined above. It is in practice also exceedingly difficult to isolate individual diffraction spots in the $1T_2$ pattern for dark field work because there are so many. Further it has to be noted that there exists for the 1T structure an inter-sandwich stacking problem which is not present for the 2H structure. Stacking of the structure and of its CDW affects the mutual DC interactions, their alignment, and hence the way, and indeed the possibility, of viewing the array. Finally, the diffraction information indicates that the DC spacing in the array being sought is going to be only $\simeq 75$ Å, i.e. just six CDW wavelengths. Accordingly for any but the narrowest of DC phase-slip boundaries the contrast will be further impaired.

In the past, our attempts to index the diffraction pattern of the $1T_2$ state have pointed to the 18-by-5 rotated superstate, discommensurately related to the 18-by-6 ($6 \times \sqrt{13}$) base [12]. The turn angle for the 18-by-5 state is 11°55′, and the modulus of the effective CDW q-vectors becomes $0.2864|\boldsymbol{a}_0^*|$. Although the latter value differed somewhat from what the diffraction would appear to suggest ($\simeq 0.285|\boldsymbol{a}_0^*|$), perhaps this was to be explained by significant structural modification in the region of the DCs. Comparison of figure 18 in [2], which provides a careful rendering of the experimental electron diffraction pattern (see figure 7(ii) there—reproduced now as figure 1), with the diffraction pattern for the 18-by-5 condition given in figure 16 of [12] indicates the level of discrepancy. To facilitate a more detailed comparison, analogous segments of these two patterns appear now in figures 2 and 3. The small decorating triangles of spots that characterise the diffraction are, while being of the correct general size and location in the 18-by-5 pattern, in somewhat the wrong orientation. In particular in the experimental pattern, note that (i) triangles in the inner ring of unshaded triangles do not point to the origin but are rotated by $\simeq 6°$†, (ii) the shaded and unshaded triangles are as a result not directly back-to-back, but laterally staggered, and (iii) the arm in a shaded triangle running towards its strong spot points almost but not quite at the strong spot in a neighbouring shaded triangle.

Besides these 'technical' problems with the accommodation of the diffraction pattern detail, it was not understood why if the drive to $\sqrt{13}\,a_0$ commensurability is so strong that the system rotates by 13°54′ to gain the $1T_3$ state—and to hold this commensurability to 460 K in 1T-$TaSe_2$— should the process in the sulphide come to a halt after the apparent substantial rotation of 11°54′, only 2° short of full lock-in.

† The triangle sides take the orientations 3-by-2, as close as could be measured [2].

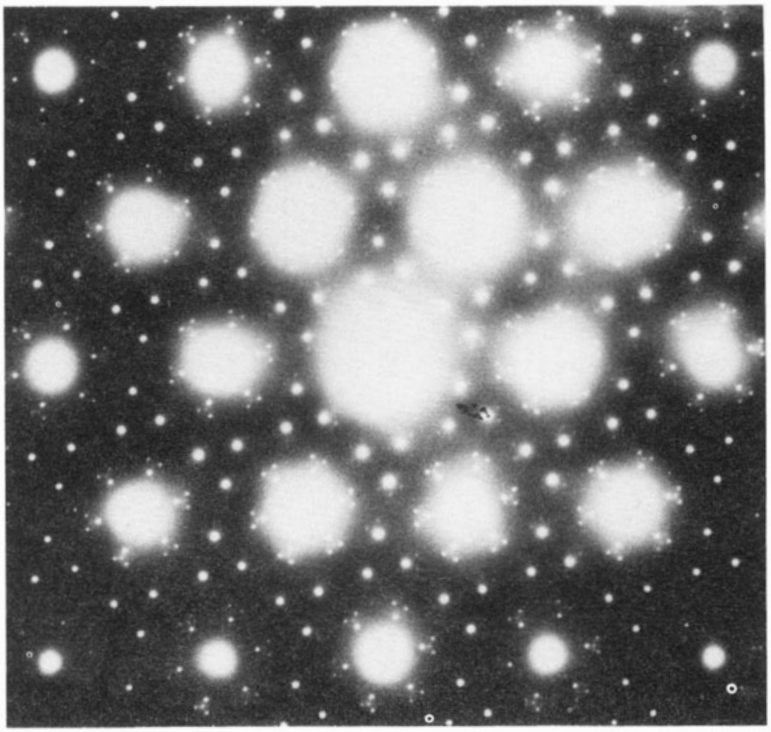

Figure 1. Well centred electron diffraction pattern of anticlockwise variant of $1T_2$ room temperature, 'quasi-commensurate' CDW state of 1T-TaS_2. See accurate drawing of repeat segment of same in figure 2. Small triangles of spots decorate $a_0^*/\sqrt{13}$ lattice points of commensurate $\sqrt{13}\,a_0$ $1T_3$ low temperature CCDW state. Many of weak spots actually out of basal plane, and evident here only by projection, due to crystal film being only ≈800 Å thick. Orientations of edges of decorating triangles very close to 3-by-2.

The resolution to all the above difficulties is now to be extracted from the very recent scanning tunnelling microscopy results obtained by Wu and Lieber [1]. Previous work of this type [13] had continued to fail to reveal the discommensurate character of the $1T_2$ phase. Such a state of affairs was particularly disappointing given that STM is a surface sensitive probe, and so one that might be expected to circumvent the *c*-axis stacking problem of the 1T system. (Already it was established from LEED [14] and He atom scattering [15] that the CDW does indeed persist strongly into the outermost sandwiches of a crystal.) Reasons for the success now finally gained by Wu and Lieber are probably three-fold: (i) use of good quality crystals leading to good quality cleavage, (ii) obtaining very wide area scans, and (iii) no Fourier massaging of the final image. The answer to be extracted below from this new STM work is that the $1T_2$ state is associated not primarily with the 18-by-5 state, but with a $19\frac{2}{3}$-by-$2\frac{2}{3}$ rotated condition having some features in common with the 18-by-5 state.

As we shall see, the new state identified above constitutes an effective half-way stage *en route* to full $\sqrt{13}$, 3-by-1 commensurability. The form displayed by the new structure across its discommensurate boundaries does not seem to offer any obvious advantages over the various other neighbouring possibilities open to consideration, and its adoption would appear rather to be a matter of stacking. The $19\frac{2}{3}$-by-$2\frac{2}{3}$ state will now be shown to match fully both the early diffraction data and the new STM images.

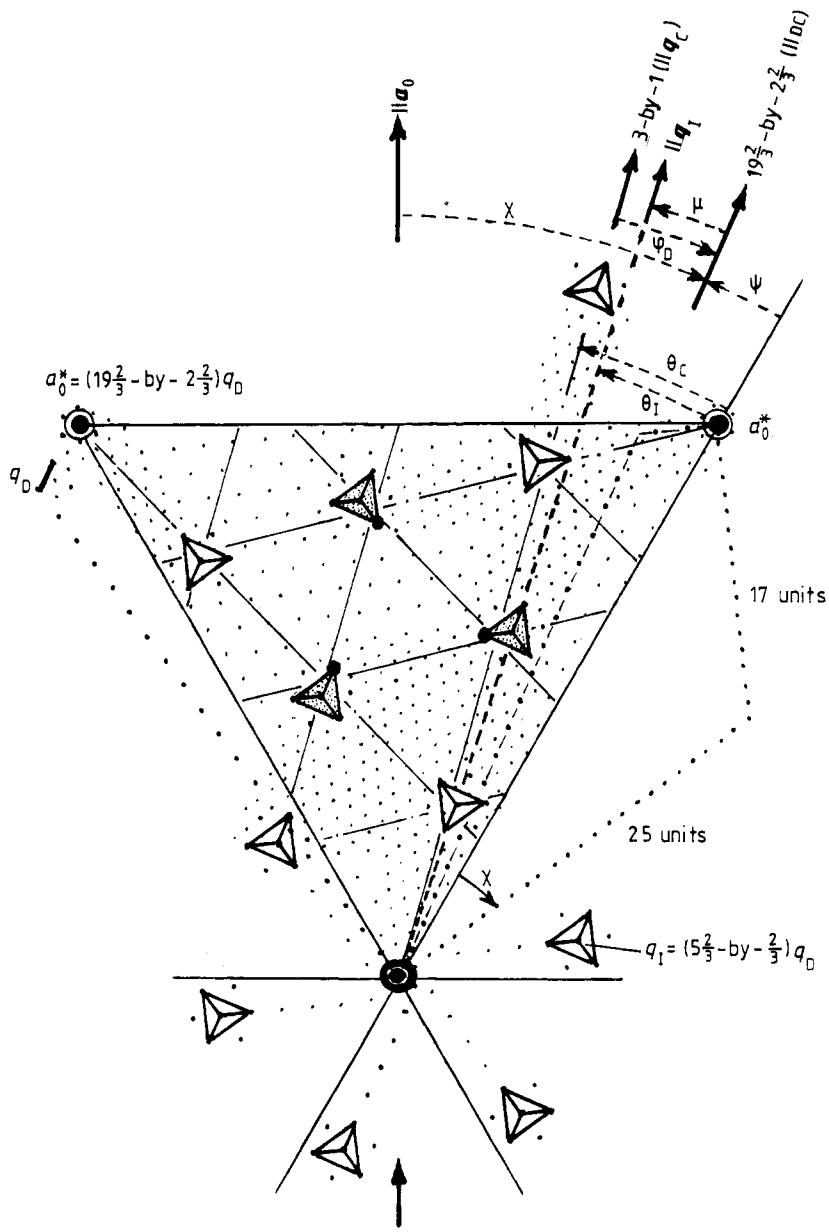

Figure 2. Electron diffraction pattern for $1T_2$-TaS_2, carefully drawn up from figure 1 (and subsequently calculated below). State label $19\frac{2}{3}$-by-$2\frac{2}{3}$ generates the fine mesh of lattice points (q_D). As in all figures a_0 for basic CdI_2 lattice defines 'vertical' on page. In addition to a_0^* lattice, figure also features reciprocal lattice for $\sqrt{13}$ a_0 CCDW. All figures are for anti-clockwise-rotated CDW variant. Numerical values for lengths and angles in this and later similar figures are collected into table 2 at the end of the paper for ease of comparison. The various angles themselves are defined there in table 1.

$$q_I = 0.2853|a_0^*| \qquad \theta_I = 11°46' \qquad \psi = 6°16\tfrac{1}{2}'.$$

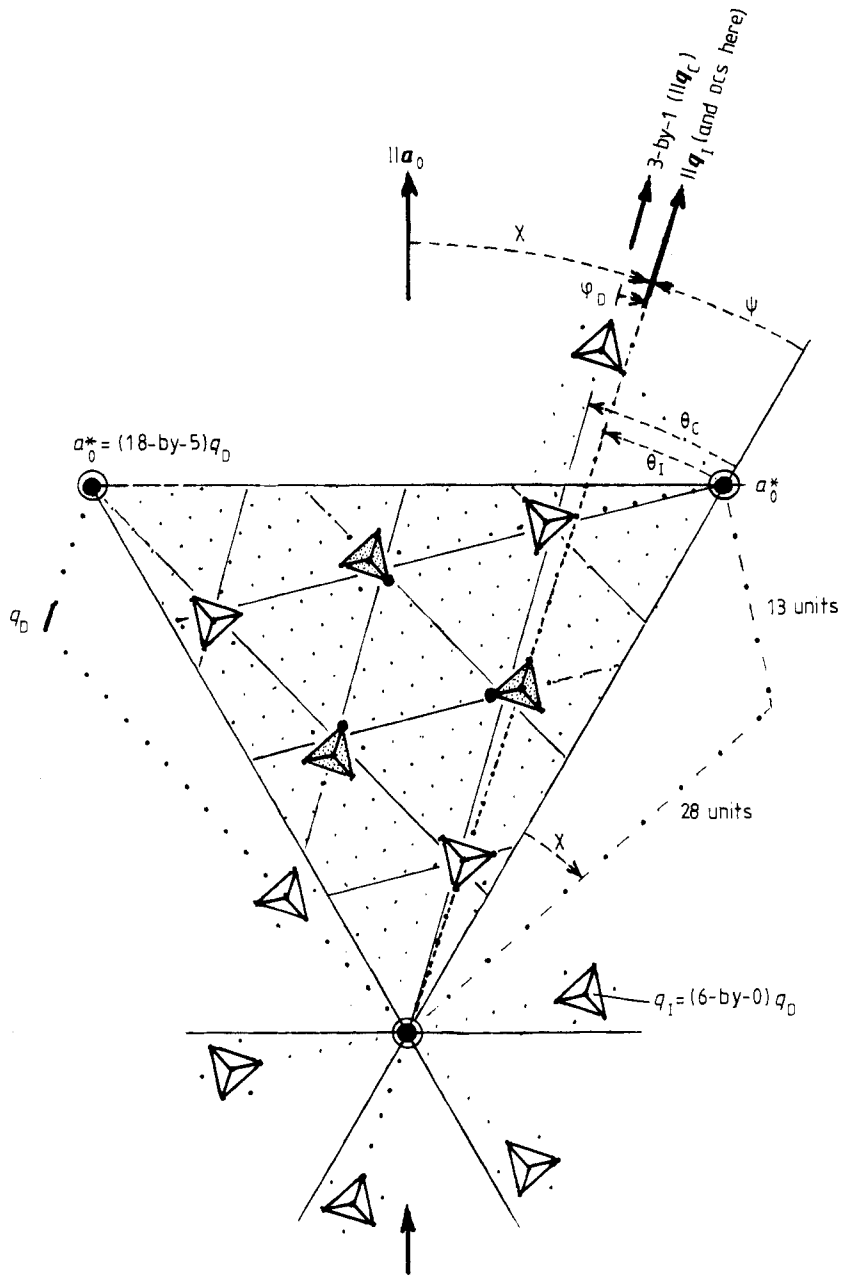

Figure 3. Similar figure to figure 2 for the 18-by-5 state discussed in reference [12] in connection with $1T_2$-TaS_2. Note small decorating triangles now point directly to origin.

$$q_I = 0.2863|a_0^*| \qquad \theta_I = 11°56' \qquad \psi = 11°56'.$$

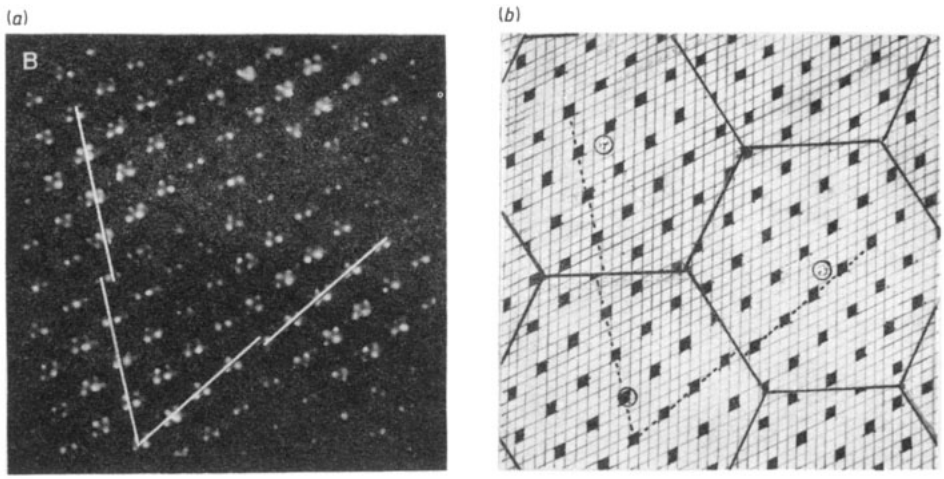

Figure 4. (*a*) High magnification STM image [1] resolving atomic positions in outermost distorted sulphur atom plane in $1T_2$ condition. The jog between domains here is of magnitude a_0, and is directed such that $q_1 > q_C$ ($= 0.2773|a_0^*|$).

(*b*) Rendering of the experimental data, with slight modification in the atom positions to bring them onto a simple lattice. As for figure 5, the tunnelling current is not passing perpendicular to foil (or the STM *x* and *y* piezo-electric scans are not performing equivalently), so that the basic lattice angle appears to be 63° here. The lozenge shape featuring in this image is of uniform orientation in all domains, and in subsequent figures it is uniformly converted to hexagonal form for the Ta sheet immediately below the S sheet being viewed here. The precise positions of the domain centres and domain walls in this figure have been added in the light of the analysis which follows.

2. Description of the $19\frac{2}{3}$-by-$2\frac{2}{3}$ $1T_2$ state

The nature of the jog or displacement vector associated with the $1T_2$ discommensurate state is evident from the high resolution scanning tunnelling image of figure 4 obtained by Wu and Lieber [1]. As will be seen later in figure 6, it is the same one upon which the 18-by-5 state is based. It increases the length of the effective wavevector relative to that for $\sqrt{13}$ commensuration, whilst at the same time it acts to reduce the effective turn angle from the full $\sqrt{13}$ lock-in value (one refers to 18-by-6 or 6(3-by-1) in the case of the 18-by-5 state). What is lacking in figure 4(*a*) is a proper identification of the domain centres. That can be gained by carefully examining the wide-area STM scan provided in figure 5. The latter figure has been rotated relative to the orientation in which it was presented by Wu and Lieber in order to bring it into the same orientation as figure 4 (namely a_0 vertical). In order also to make explicit the various relationships, the figure is shown framed firstly by a hexagon in the orientation of the discommensurations, secondly by a hexagon in the orientation of the CCDW within the commensurate patches, and thirdly by a hexagon parallel to the atom rows of the underlying crystal lattice. As was noted by Wu and Lieber the patch centres in this discommensurate array do not in fact lie in a direction particularly close to the $\sqrt{13}$ direction, but instead lie in one that approximately bisects the 13°54′ angle between CCDW and basic lattice.

The above unification in orientation of figures 4 and 5 has been gained by making proper identification of the patch centres; these clearly do not fall at the points suggested by the bar ends in figure 4(*a*). A first requisite is to identify the nature of the repeat motif

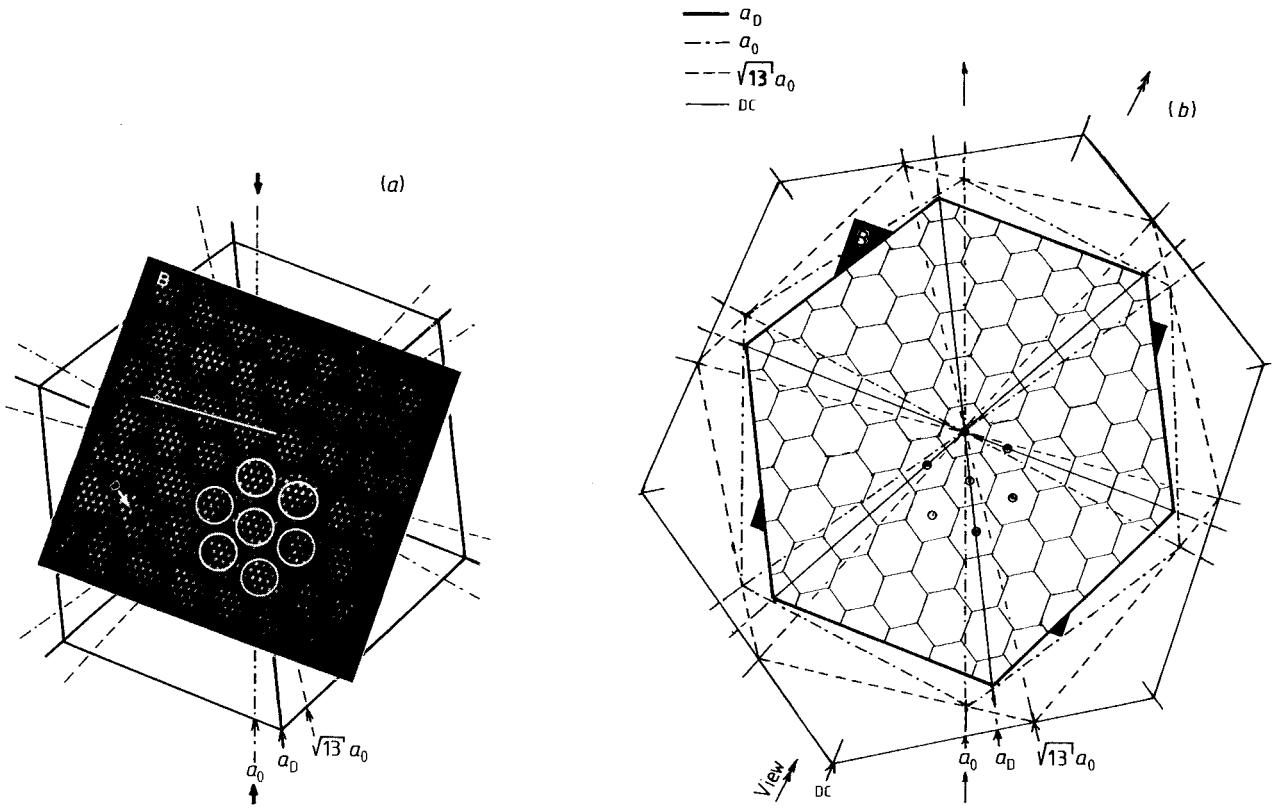

Figure 5. (*a*) Wide-area low magnification STM scan from [1] for $1T_2$-TaS_2. The 'spots' now are the entire lozenges featuring in figure 4. The discommensurate domains, strongly in evidence here, are 70 Å across. The plate has been rotated to bring it into what the present analysis identifies as being of common orientation with the other figures (namely a_0 'vertical'). The plate exhibits an even stronger 'perspective' effect than figure 4, and to 'normalise' should be viewed from the 'south west' at about 50° from horizontal. (*b*) Overlay of domain boundaries for figure 5(*a*), coming from subsequent analysis. Surrounding large hexagons identify (working from outermost inwards), (i) $1T_2$ DC orientations, (ii) $\sqrt{13}$ CCDW orientations, (iii) $\boldsymbol{a}_0$ basic lattice directions, (iv) domain lattice orientation $\boldsymbol{a}_D$. Remember corresponding reciprocal lattice directions rotated by 30° in hexagonal system (see table 1).

showing up strongly in the STM images. The four atom, diamond motif of figure 4 is taken to reflect sites in the outermost sheet of the sulphur atoms, displaced upwards by the contraction of the 13-atom Ta star centre in the sheet below. Here four atoms rather than three are presumed to show up strongly because of the overall breaking of the hexagonal symmetry through a stacking sequence that is linear rather than helical. A unique orientation is then taken to hold for the rhomb throughout the experimental pattern. Hence, in the patterns of the present paper, one is able to transform all rhombs

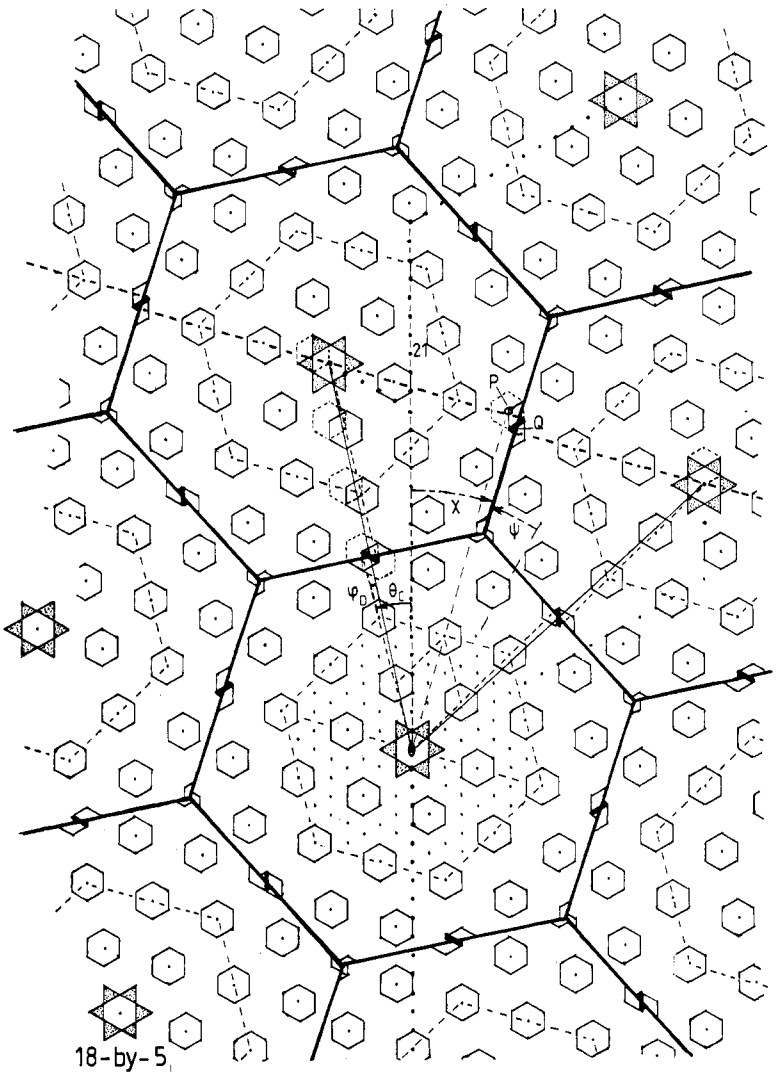

Figure 6. Regular DC array based on rotated contraction from full lock-in of 6(3-by-1) to 18-by-5. The cyclic array of unit phase-slip vectors across the DCS is indicated. The lozenges of the sulphur sheet have been transformed to the hexagons of the tantalum atom sheet. The central patch of each domain contains twelve $\sqrt{13}\,a_0$ cells. All domains are similarly centred, and the centres are shifted by only $1a_0$ from the $\sqrt{13}$ CCDW axes. P marks wavefront normal to the sixth CCDW wavefront from origin, and Q is a corresponding point (here at jog centre) for the effective wavefront defining q_1 in the quasi-commensurate condition. The figure should be closely examined in conjunction with figure 3.

via a common mode of expansion into a hexagonal motif. This should then portray the primary CDW activity within the underlying Ta sheet. (The full 13-atom star is used only where necessary to draw attention to the domain centres.)

Careful examination of figure 5 will reveal that successive domains are not always centred on a metal atom cluster. The domain centres shift steadily from one string of stars to the next. Actually the pattern is of sufficient regularity as to suggest a required repeat span of three domains. From the STM data alone, however, it is impossible to proceed further. It is now necessary to combine the STM information with the diffraction information of figures 2 and 3.

In figure 6 is portrayed the 18-by-5 structure, which as we have seen earlier has the correct domain size ($\simeq$70 Å), the correct DC jog vector, and a general rotation which comes close to matching the available diffraction data. However, the 18-by-5 condition of figure 6 sees all its domains identically centred upon a Ta cluster. Such a defect—essentially one of rotation—is matched in the diffraction results by the discrepancies noted already between figures 2 and 3 (which relate respectively to the experimental diffraction pattern and to the one that would derive from the 18-by-5 array). In the latter pattern it is to be seen that the inner 'decorating' triangles point directly at the neighbouring basic a_0^* spots, and the shaded and unshaded pairs of triangles then fall exactly back-to-back. In the original diffraction work of [2] it was observed that the orientation of the sides of the triangles in fact take (as closely as could be measured) the skewed orientation 3-by-2. This necessitates that in order to accommodate the observed spots the diffraction mesh must be very fine indeed: a three-fold increase in mesh density is required over the 18-by-5 situation.

Such a change calls for a $\sqrt{3}$ times linear expansion in the cell size over the 18-by-5 cell made in conjunction with a 30° rotation. The means of accomplishing this is to push the domain centre back from the 18-by-5 position towards the primary atom string. The shift is towards the neighbouring string of CDW charge centres to take up the three-star centroid position $19\frac{2}{3}$-by-$2\frac{2}{3}$. The new state is shown in figure 7. Its effective CDW wavevector is intermediate in length between those corresponding to the 18-by-5 state and its $\sqrt{13}$ commensurate partner, 18-by-6. As has been noted above, for this 'non-integral' rotation the patch centres in the $19\frac{2}{3}$-by-$2\frac{2}{3}$ direction will now fall in a three-fold sequence

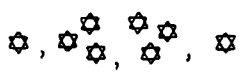

and the true unit cell is rotated by 30° and is $\sqrt{3}$ times linearly expanded. The diffraction patterns of figures 2 and 3 support the necessity for this cell enlargement. We see in figure 7 that the real space cell vector is directed not in the $19\frac{2}{3}$-by-$2\frac{2}{3}$ orientation to 59-by-8, but in the 30° rotated direction to 17-by-25. This now makes the derived diffraction pattern of figure 2 agree exactly with experimental readings. The diffraction results imply that the *c*-axis stacking of the DC array is likewise in the same $\sqrt{3}$ orientation; an ABC three-sandwich stack of the honeycomb arrays then produces no additional projected basal plane spotting. With this arrangement, patch centres of maximal CDW activity sit above and below nodes in the DC arrays in flanking sandwiches where CDW activity is at a minimum. This ABC stacking mode for the honeycomb DC arrays of successive sandwiches must contribute significantly to the low visibility of the DCs under the EM imaging. By contrast, for the 2H case the DCs in successive sandwiches stack directly above each other.

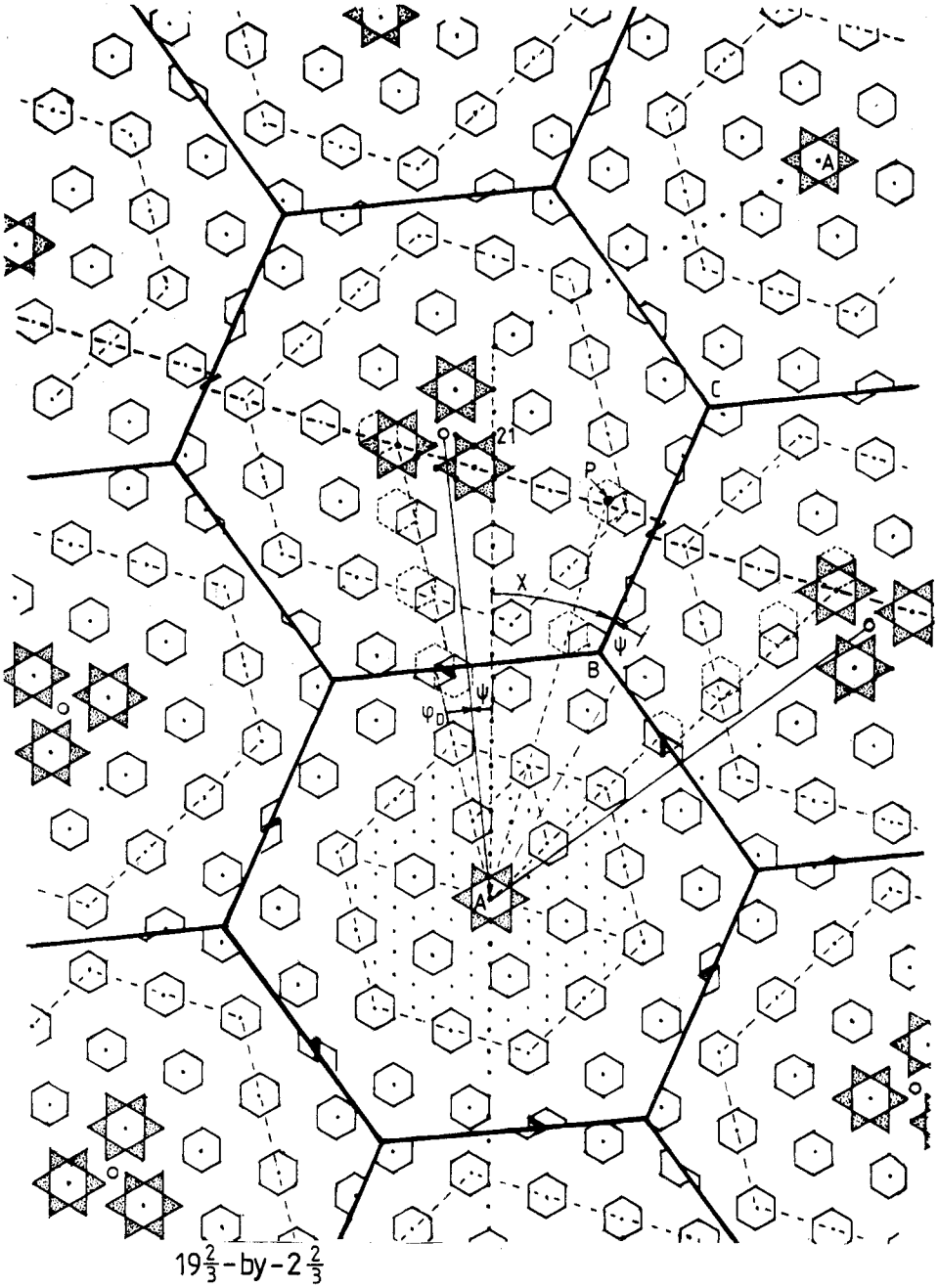

Figure 7. Figure corresponding to figure 6 but for actual $19\frac{2}{3}$-by-$2\frac{2}{3}$ condition in $1T_2$-TaS_2. Figure should be compared with STM images in figures 4 and 5, and with diffraction pattern of figure 2. Unlike case for 18-by-5, this $19\frac{2}{3}$-by-$2\frac{2}{3}$ state does not have all domains similarly centred. Also the domain centres are significantly rotated away from the $\sqrt{13}$ CCDW direction (i.e. $\mu = \theta_1 - \psi \neq 0$). However q_1 and θ_1 acquire values very similar to values in the 18-by-5 condition (see table 2), For $a_0 = 3.345$ Å the domain diameter is 70-66 Å. The real unit cell runs from A to A (i.e. 25-by-17), and covers three DC domains. Subsequent TaS_2 layers take a three-fold ABC stacking sequence.

In the next section additional details and reasons for adoption of the above identified $1T_2$ state will be given.

3. The nature and origins of the $1T_2$ state

The first feature resolved about the discommensurate $1T_2$ state by the wide-area scanning tunnelling images (such as figure 5) is that the material is strongly discommensurate. The amplitude of the CDW drops markedly in the phase-slip boundary. Moreover the boundary itself is quite narrow—namely <16 Å, or $1\frac{1}{3}$ CDW wavelengths. Nonetheless, this still means that a significant fraction of each domain lies within the boundary region because the domains themselves are only 6λ or 70 Å across. (Recall—a_0 for the underlying CdI_2 structure is only 3.345 Å, giving a $\sqrt{13}$ CCDW cell edge of 12.06 Å.) With central patches as indicated in figure 7, a star-centred domain holds there just 19 stars out of a total complement of ≈34, namely 56%. The $1T_2$ structure hence involves domains that are probably about as small as can stabilise a discommensurate structure, even for such narrow DCs.

The narrowness of the DCs and the drop in amplitude of the CDW in the boundary region each express a strong non-sinusoidality. This was always apparent from the diffraction pattern with its sharp high order spotting. The final product indeed is almost like a shear structure in a non-stoichiometric system (e.g. a member of the Ti_nO_{2n-1} family). The regularity of the DC array is very considerable. The degree of regularity monitors the relative balance between the ordering forces of DC–DC interaction on the one hand, and on the other, thermal disordering, pinning to defects, and self-pinning to the lattice. The present boundary geometry does not of itself appear to be an especially favoured configuration vis-à-vis the various other boundaries that might have arisen (see below). In common with all those other discommensurate structures (such as 18-by-5), which are based upon the present jog vector, the CDW star centres are separated across the DCs boundary by $3a_0$.

The STM results have also resolved the question as to whether the domains would take honeycomb or triangular form. A honeycomb array clearly permits the central patch to be appreciably larger in area relative to the surrounding boundary region in a case where, as for the present, one has small area domains.

Table 1. Definitions and interrelations of angles in direct and reciprocal space. Anticlockwise rotations signed positive. Principal reference direction 'vertical' atom row. $\boldsymbol{a}_D$ = domain centre vector; $\boldsymbol{q}_D$ = corresponding wavevector. $(11\bar{2}0)\boldsymbol{a}_D \| DC$, $\theta_I = \theta_C \pm \Delta\theta$, $\psi - \varphi_D = \theta_C$, $|\chi| + |\psi| = 30°$, $\theta_I = \psi + \mu$, (φ_R measured as φ_D, but from associated reference vector for CCDW.) Orientation m-by-n (anticlockwise variant):

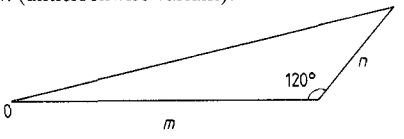

Angle	Direct space	Reciprocal space
θ_I	—	$\boldsymbol{a}_0^* \hat{} \boldsymbol{q}_{I(CDW)}$
ψ	$\boldsymbol{a}_0 \hat{} \boldsymbol{a}_D : (11\bar{2}0)\boldsymbol{a}_0 \hat{} DC$	$\boldsymbol{a}_0^* \hat{} \boldsymbol{q}_D$
φ_D	$\boldsymbol{a}_{CCDW} \hat{} \boldsymbol{a}_D$	$\boldsymbol{a}_{CCDW}^* \hat{} \boldsymbol{q}_D$
χ	$(11\bar{2}0)\boldsymbol{a}_0 \hat{} \boldsymbol{a}_D : \boldsymbol{a}_0 \hat{} DC$	$(11\bar{2}0)\boldsymbol{a}_0^* \hat{} \boldsymbol{q}_D : \boldsymbol{a}_0^* \hat{} (11\bar{2}0)\boldsymbol{q}_D$
μ	—	$\boldsymbol{q}_D \hat{} \boldsymbol{q}_I$

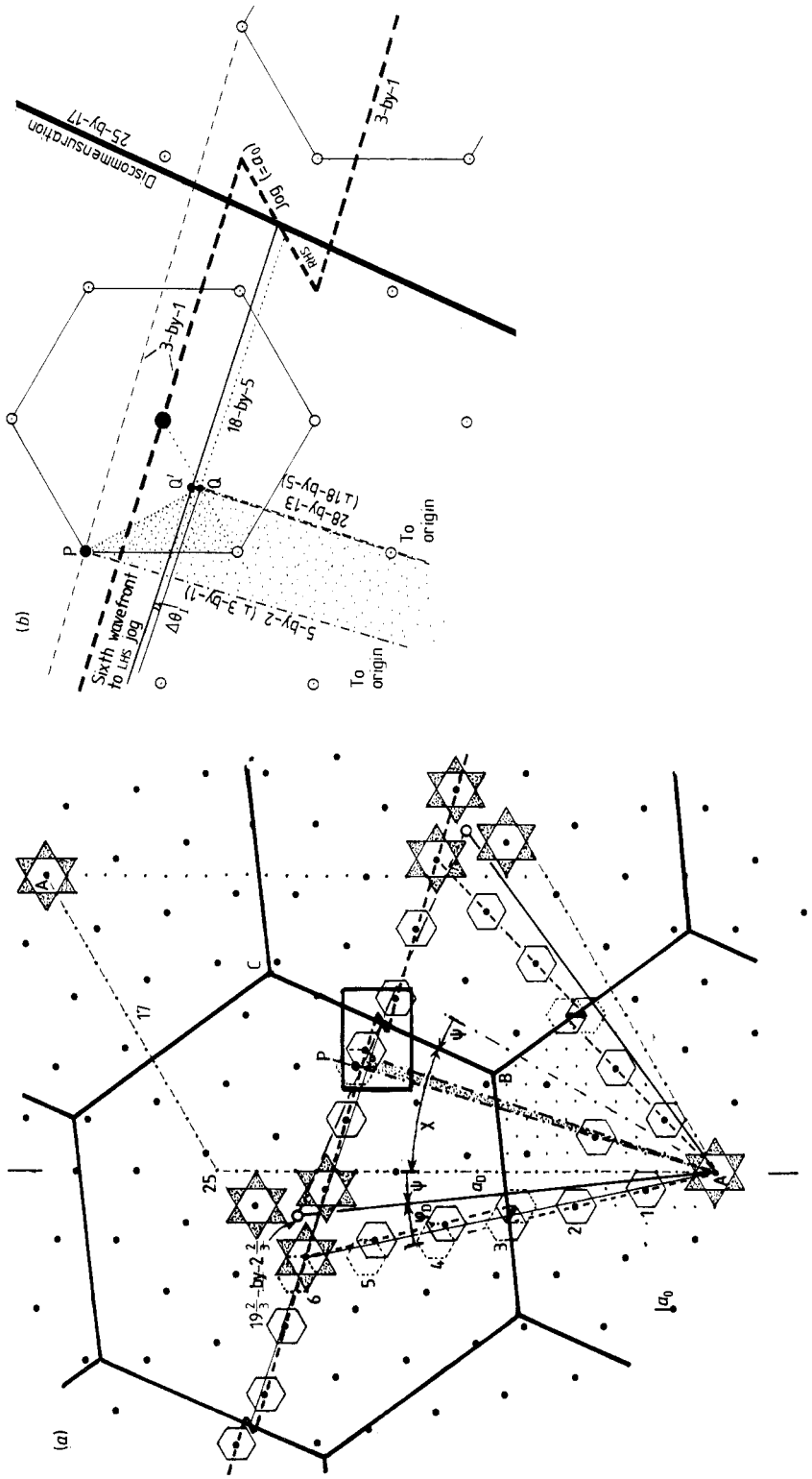

Figure 8. (*a*), (*b*) Closer examination of the 1T, $19\frac{2}{3}$-by-$2\frac{2}{3}$ state in the vicinity of the sixth wavefront from the origin. The small rectangle on figure 8(*a*) shows the area portrayed in figure 8(*b*). The narrow shaded area indicates the turn in wave vector orientation from q_c to q_l. Between the 18-by-5 and $19\frac{2}{3}$-by-$2\frac{2}{3}$ states the wave normal position shifts from Q to Q′, where PQ′/PQ = $\frac{10}{11}$, and $\Delta\theta_l = 0°10'$.

Finally we shall consider an aspect raised by McMillan concerning whether the discommensurations set themselves perpendicular or parallel to the effective CDW wavevector. The answer for the $19\frac{2}{3}$-by-$2\frac{2}{3}$ state is neither. The choice considered by McMillan was for a discommensurateness of the hexagonal system introduced only along high symmetry directions (i.e. along the axis of the cell or the 30° rotated $11\bar{2}0$ direction). The present case is one from a more general class of rotated discommensurate options.

In figure 8 is presented the central region of figure 7 emphasising the geometrical interrelation between the domains and the effect on the wavefront normal for the discommensurate condition of the $19\frac{2}{3}$-by-$2\frac{2}{3}$ state. The various angles used in subsequent numerical analysis of this, and the similar figures to follow, are marked on figure 8(*a*)

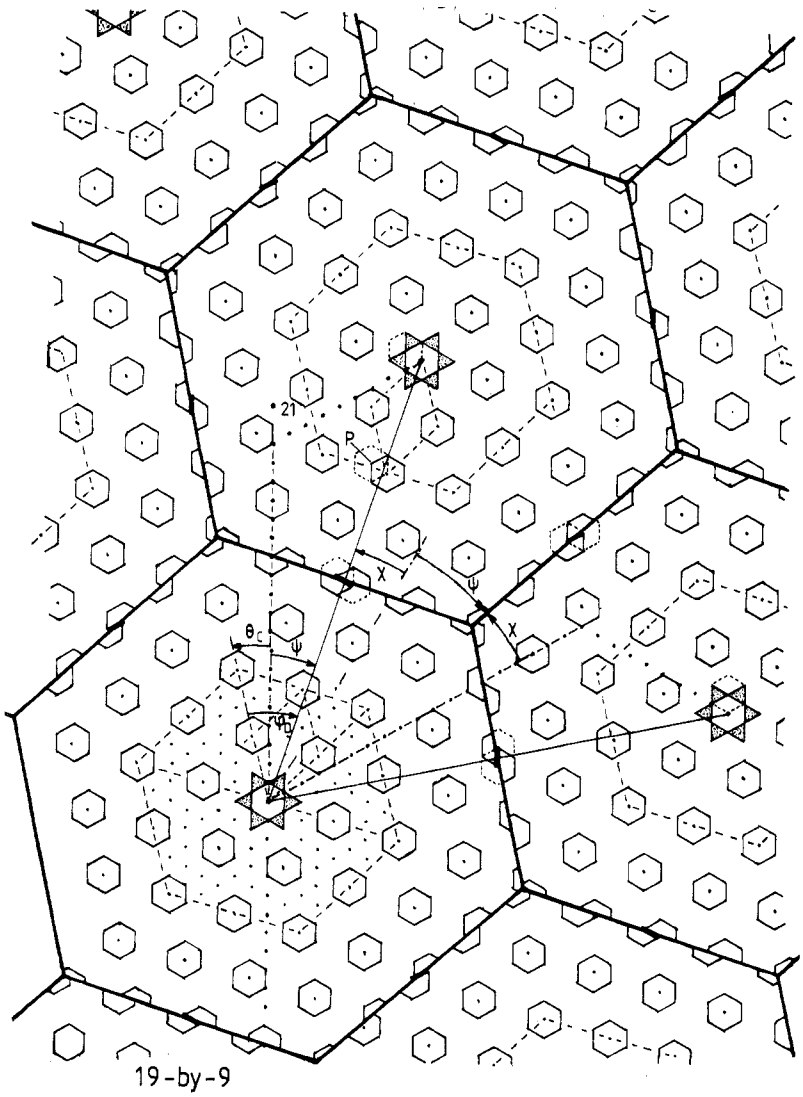

Figure 9. Case of the 19-by-9 $\varphi_D \simeq 30°$ DC structure, where q_I approximately perpendicular to DC, unlike the 18-by-5 $\varphi_D \simeq 0°$ case, for which q_I is approximately parallel to DC.

and identified and interrelated in table 1. Some of the angles such as φ_D and χ are of greater use when constructing the real space figures, while others like μ and θ_I are of more significance when dealing with the diffraction patterns. The geometry of these states is automatically complicated because (i) the CCDW is rotated WRT the basic lattice, (ii) the DC domain array is rotated WRT the CCDW, (iii) for $19\frac{2}{3}$-by-$2\frac{2}{3}$ the sub-cell is rotated WRT the true cell, and finally (iv) for each of these hexagonal lattices there exists the inevitable 30° rotation between real and reciprocal space.

Figure 8(*a*) concentrates on the sixth wavefront from the origin. P marks the wave-normal to this CCDW wavefront. For the incommensurate/discommensurate state, $19\frac{2}{3}$-by-$2\frac{2}{3}$, the corresponding point, Q′, does not fall at a particularly simple geometric position. For the simpler 18-by-5 state the wave-normal is to the special point Q. Figure 8(*b*) is an accurate expansion of the situation holding for the $19\frac{2}{3}$-by-$2\frac{2}{3}$ state in the vicinity of the wave-normal position and the unit jog at the right hand side of the domain. The wave-normal length and orientation give of course the effective wavevector for the discommensurate condition. While it is possible to evaluate $\boldsymbol{q}_I$ in magnitude and orientation directly from this real space view, it is in fact much easier to proceed in reciprocal space. Because I would like to do this on a somewhat more general basis than simply for the $19\frac{2}{3}$-by-$2\frac{2}{3}$ state, I would ask the reader to study carefully the following pairs of figures,

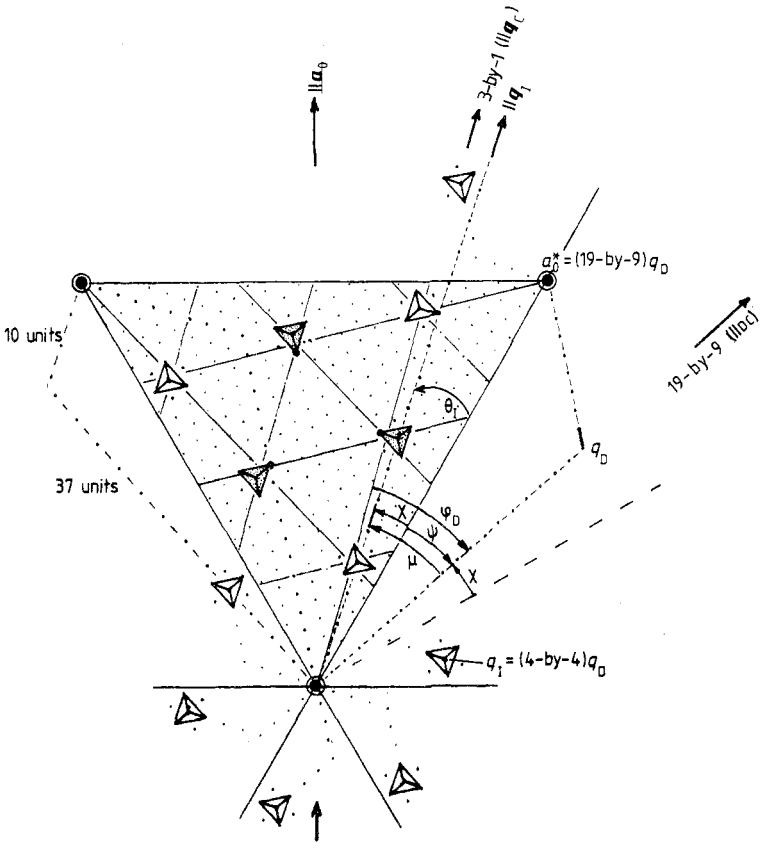

Figure 10. Corresponding diffraction pattern to figure 9. In 19-by-9, $\mu = 30°$, while in 18-by-5, $\mu = 0°$. The small triangles are now much more strongly rotated than in figure 2 for the $19\frac{2}{3}$-by-$2\frac{2}{3}$ case.

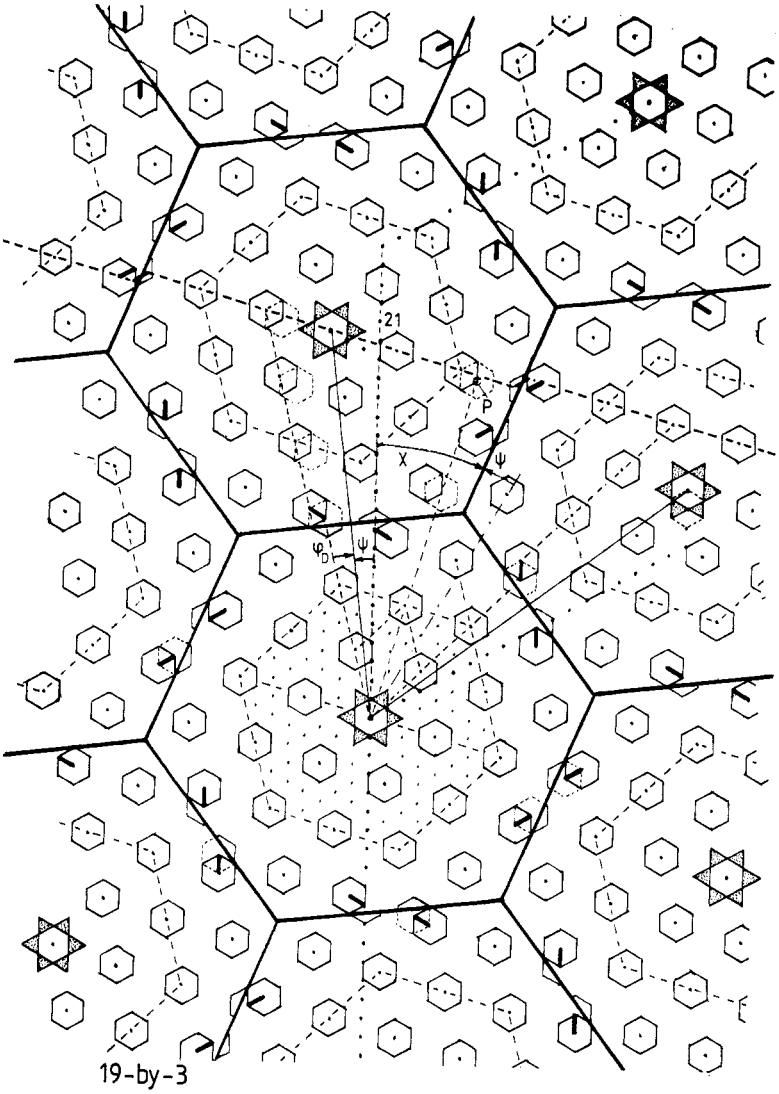

Figure 11. 19-by-3. An example of a DC-array for which $\lambda_I > \lambda_C, q_I < q_C, \theta_I > \theta_C$. Also unlike $1T_2$-TaS_2 all domains are equivalent. However, like the $19\frac{2}{3}$-by-$2\frac{2}{3}$ state, ψ is $\simeq \theta_C/2$. Compare with corresponding diffraction pattern of figure 12.

relating to real and reciprocal space:

figures 3 and 6, for a simple, axial-type ($\mu = 0°$), situation, 18-by-5;
figures 9 and 10, for an $11\bar{2}0$-type ($\mu = 30°$) example, namely 19-by-9;
figures 11 and 12, for an intermediate but integrally sited domain centre, where all domains are star centred, 19-by-3;
and figures 2 and 7, for the more general situation of $19\frac{2}{3}$-by-$2\frac{2}{3}$.

These various states are identified in figure 13, in which the intermediate nature of the $1T_2$ state (i.e. $19\frac{2}{3}$-by-$2\frac{2}{3}$—marked H) with respect to the $1T_3$ CCDW condition C, and X,

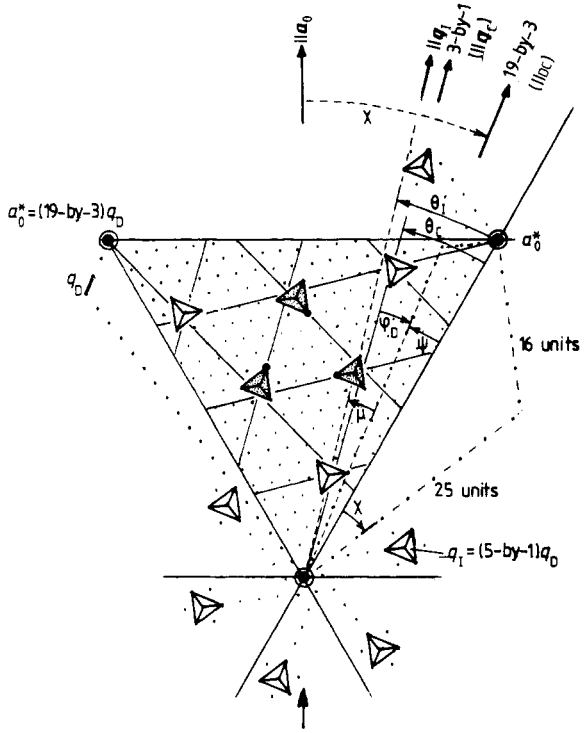

Figure 12. Diffraction pattern for 19-by-3 state of figure 11. $q_I = 0.2798|a_0^*|$; $\theta_I = 16°10'$; $\psi = 7°13'$.

the location of the corresponding charge hill in the ICDW $1T_1$ state is immediately to be seen.

A synthesis of what is to be extracted from study of the preceding figures is provided in figure 14. In figure 14 one has, for the repeat range in φ_D (0°–30°), the orientations of the 6-unit jog vectors (a to e) in relation to the range of the DC orientations. The important question then for any particular state is whether the given combination implies a decrease in either or both of the magnitude and the rotation of the effective wavevector vis-à-vis the $\sqrt{13}$ commensurate condition. The four cases are specified via the quadrant symbols I to IV.

For the $19\frac{2}{3}$-by-$2\frac{2}{3}$ state we have an 'aI' condition: i.e. $q_I > q_C$ and $\theta_I < \theta_C$. The values are $q_I = 0.2853\,|a_0^*|$ and $\theta_I = 11°46'19''$ compared with $q_C = 0.2773|a_0^*|$ and $\theta_C = 13°53'52''$ for the $\sqrt{13}$ state. These values and all those appearing in table 2 may be quoted to any desired accuracy since they arise from specific geometries. The most convenient route to filling out this information is (for the $1T_2$ case):

(a) in $19\frac{2}{3}$-by-$2\frac{2}{3}$ 120° triangles (units of a_0)—see figure 7,

(i) $a_D = 21.126a_0$ (ii) $\psi = 6°16'33''$

(iii) $\varphi_D = \psi - \theta_C = -7°37'20''$ (iv) $\chi = 30° - \psi = 23°43'27''$

(b) then in $5\frac{2}{3}$-by-$\frac{2}{3}$ 120° triangles (units of q_D)—see figure 2,

(i) $q_I = 6.0277|q_D|$ (ii) $\mu = 5°29'49''$.

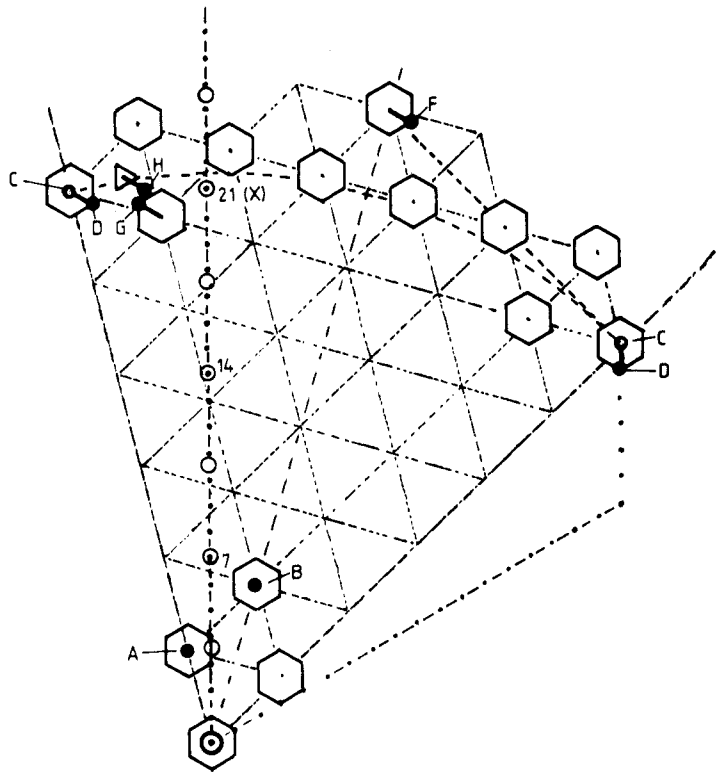

Figure 13. Relative sitings of the various domain centre positions considered in this paper C = 6A = 6(3-by-1) (B = 30° complement to A: 5-by-2); D = 18-by-5; F = 19-by-9; G = 19-by-3; H = $19\frac{2}{3}$-by-$2\frac{2}{3}$. In high temperature ICDW state ($1T_1$), q_I is such that charge hills fall very close to multiples of $3.5a_0$. Hence state H of $1T_2$ constitutes exact half-way house in rotation from $1T_1$ to $1T_3$ condition (marked by X and C respectively).

But $q_D = (a_0/a_D)|\boldsymbol{a}_0^*| = (1/21.126)|\boldsymbol{a}_0^*|$, so that $q_I = 0.2853|\boldsymbol{a}_0^*|$.
Also $\theta_I = \mu + \psi = 11°46'20''$.
As $a_0 = 3.345$ Å, the domain diameter $a_D = 70.66$ Å.

Note χ, the discommensuration orientation angle, gives also the small triangle edge orientation in the diffraction pattern. Empirically this was measured [2] to take orientation 3-by-2; i.e. 23°24'47", or less than a third of a degree from the above calculated value of χ. ψ is the '6°' turn reported by Wu and Lieber. All these quantities are then in full agreement with experiment. Note from table 2 how close the above values of q_I and θ_I are to those for the 18-by-5 state. The latter too is of type aI and relates to the sixth wavefront from the origin. What differentiates the two states are of course the values of φ_D or ψ.

The above figures all refer to the anticlockwise rotated $\sqrt{13}$ CCDW variant, and each is for a jog vector of $\boldsymbol{a}_0$. The only other distinct DC structures possible in $\sqrt{13}$-based systems would derive from jogs of $2\boldsymbol{a}_0$ ($\equiv$1-by -1). The STM results show directly that in 1T-TaS_2 we are dealing with jogs of $1\boldsymbol{a}_0$.

In all the above figures, hexagonal symmetry is preserved through a cyclic sequence of jog vectors. By contrast when only one (or two) of the q-vector components are being discommensurately modified this symmetry is broken, and one passes over into a 'stripe

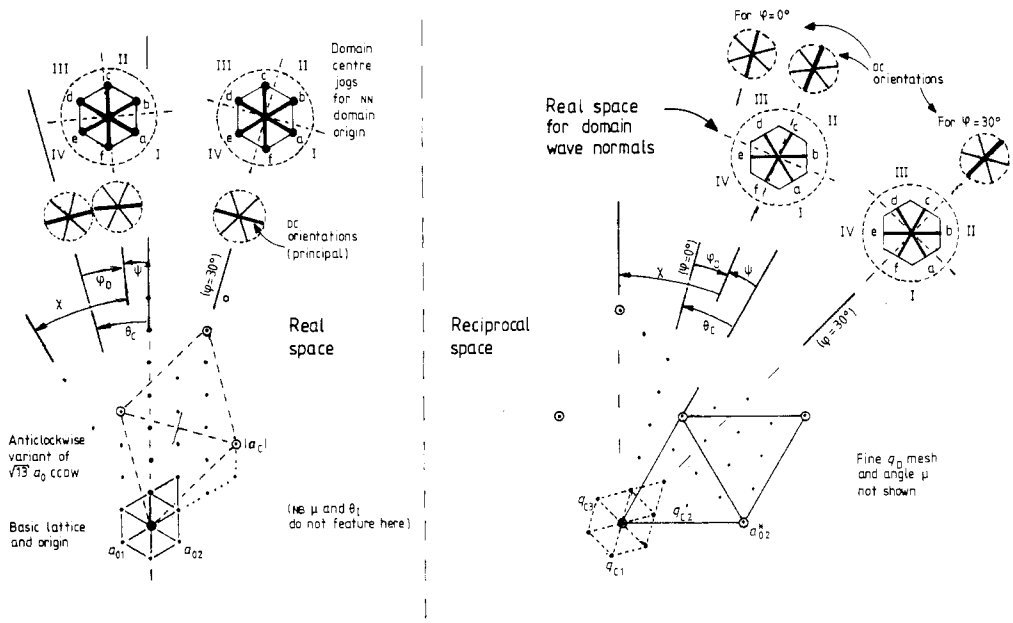

Figure 14. Summary of geometries of preceding rotated discommensurate hexagonal structures making direct comparison between various angles in both real and reciprocal space representations. For comparative definitions see table 1: $|\psi| + |\chi| = 30°$; $\psi - \varphi_D = \theta_C$; $\theta_I = \mu + \psi$. Note in the reciprocal space diagram the fine mesh corresponding to a_D is not shown. This mesh fixes angle ψ (or φ_D). For $\varphi_D = 0°$; DC $\perp$ a_{CCDW}—i.e. DC$\|q_C$ approximately. For $\varphi_D = 30°$; DC$\|a_{CCDW}$—i.e. DC $\perp$ q_c approximately. The unit jog vector across the 'principal' DC (which is the perpendicular bisector of the domain centre defining vector) can take on one of six orientations, a to f. The resulting structure types I to IV are defined through the combination of this jog vector and angle φ_d (or ψ), through the quadrant figure

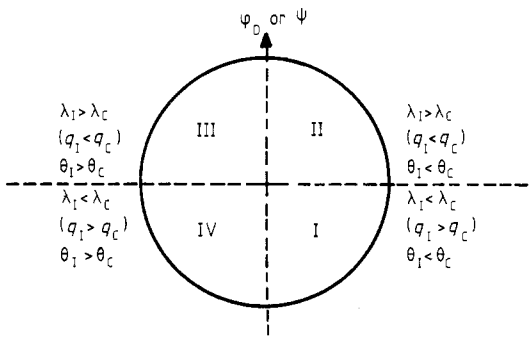

phase'. Such a situation was first detected for the 2H phase upon warming between 90 K and 112 K [16, 6(*a*)], but subsequently a similar type of behaviour was confirmed for the 1T polymorph between ≈220 K and 273 K [17]. Probably the stripe phases are metastable, although the latter reversion temperature to the $1T_2$ phase is a well-defined one—a point returned to below.

The $19\frac{2}{3}$-by-$2\frac{2}{3}$ state is a clear half-way house between the axial ICDW state $1T_1$ and the $\sqrt{13}$ CCDW $1T_3$ state (as can be seen in figure 13). For $1T_1$, $q_I = 0.288|\boldsymbol{a}_0^*|$. This drops to 0.2853 in $1T_2$ and finally to 0.2773 in $1T_3$. Large amplitude CDWs are very incompressible and so this represents a considerable energy adjustment to the lattice. For the

Table 2. Examples of discommensurate superlattices based on (anticlockwise variant of) $\sqrt{13}\,a_0$ CCDW. $\sqrt{13}$ cell edge orientation is 3-by-1; 30° complementary orientation is 5-by-2. For a $\sqrt{13}$ CCDW, $a = \sqrt{13} \times 3.345 = 12.061$ Å; $|a^*| = |q_C| = [a_0^*/\sqrt{13}] = 0.27731 a_0^*|$; $\theta_C = 13°53'52''$. (i) Orientations and angles measured WRT basic lattice (except ϕ which is WRT CCDW cell edge). Principal reference direction is 'vertical' atom row. Anticlockwise angles 'positive'. (ii) $\psi - \phi_d = \theta_c = 13°54'$; $\psi + \mu = \theta_1$; $|\psi| + |\chi| = 30°$. (iii) Unit jog vectors a–e and DC type labels defined in figure 14.

Domain centre defining vector	a_D length	DC jog vector	DC type	Commensurate reference vector	φ_D	ψ
18-by-5	20.952	a	I	18-by-6	−1°58′	11°56′
19-by-9 (clockwise)	24.758	a	I	20-by-8	−32°15′	−18°21′
19-by-3	20.652	d	III	19-by-2	−6°40.5′	7°13′
20-by-2	21.071	c	II	19-by-2	−9°11′	4°43′
$19\frac{2}{3}$-by-$2\frac{2}{3}$†	21.126	a	I	$19\frac{2}{3}$-by-$3\frac{2}{3}$	−7°37.5′	6°16.5′
in a_0 (anticlockwise except 19-by-9)	$\|a_0\|$	a_0	—	in a_0	from a_{CCDW}	—

Domain centre defining vector	Orientation of q_1	q_1 in q_D	$\|q_1\|$	θ_1	DC orientation
	μ	q_D in a_0^*	$\|q_1\|/\|q_C\|$	$\Delta\theta$	χ
18-by-5	6-by-0	6.0000	0.2863	11°56′	28-by-13
	0°00′	0.04773	1.0325	−1°58′	−18°04′
19-by-9	4-by-4	6.9282	0.2798	11°39′	10-by-37
(clockwise)	30°00′	0.04039	1.0090	−2°15′	11°39′
19-by-3	5-by-1	5.5678	0.2696	16°10′	25-by-16
	8°57′	0.04842	0.9722	+2°16′	−22°47′
20-by-2	5-by-1	5.5678	0.2642	13°40′	24-by-18
	8°57′	0.04746	0.9528	−0°14′	−25°17′
$19\frac{2}{3}$-by-$2\frac{2}{3}$†	$5\frac{2}{3}$-by-$\frac{2}{3}$	6.0277	0.2853	11°46′	25-by-17
	5°30′	0.04734	1.0288	−2°08′	−23°43.5′
in a_0 (anticlockwise except 19-by-9)	in q_D	in q_D	$\|a_0^*\|$	—	Orientation clockwise in a_0
	—	$\equiv 1/a_D$	—	—	—

† For observed structure $19\frac{2}{3}$-by-$2\frac{2}{3}$, with $a_0 = 3.345\,A$, domain spacing or diameter = $21.126 \times 3.345 = \underline{70.66\ \text{Å}}$. (Remember $19\frac{2}{3}$-by-$2\frac{2}{3}$ is subcell of true cell 25-by-17; i.e. $\sqrt{3} \times a_D$ in $(11\bar{2}0)a_D$ direction.)

corresponding diselenide the $1T_1$ q_I value is 0.286. Hence it is very interesting that the later material never samples the intermediate state, but locks-in directly to $1T_3$ at 473 K. This is caused by the larger CDW amplitude in the selenide, governed by the larger atomic mass, which leads on to lower phonon frequencies and to the higher lock-in temperature.

The high amplitude of the CDW in the 1T systems is directly reflected in the clear splitting of both Ta 4f photo-emission peaks [4]. The quasi-commensurate nature of the $1T_2$ phase of the sulphide is directly apparent here in the close relationship between $1T_2$ and $1T_3$ Ta 4f UPS signals. These signals express a Ta atom site ratio within the 13-atom supercell of 1 : 6 : 6; i.e. the CDW charge hill is centred there on a Ta atom [18]. The more complicated signal splittings seen in NMR [19], NQR [20], Mössbauer [5(a), 5(b)] and TDPAC [5(c)] work have suggested to some workers a more awkward 'seating' of the CCDW on the lattice. However, the latter hyperfine measurements are dictated by the local fields, and these incorporate a significant, low symmetry, stacking component for the high amplitude CDW. In the $1T_2$ state, the fact that there are several site types within the DC boundary regions probably just leads to some measure of signal broadening.

A remaining question to be addressed is whether the $1T_2$ state of 1T-TaS_2 is the sole intermediate DC state between $1T_1$ and $1T_3$. We have previously searched for intermediate states, both by electron diffraction [2] as a function of temperature and by capacitance dilatometry [21]. However, with the former technique it is very difficult to measure up the diffraction patterns to the required accuracy (q_I to 1 part in a 1000, and

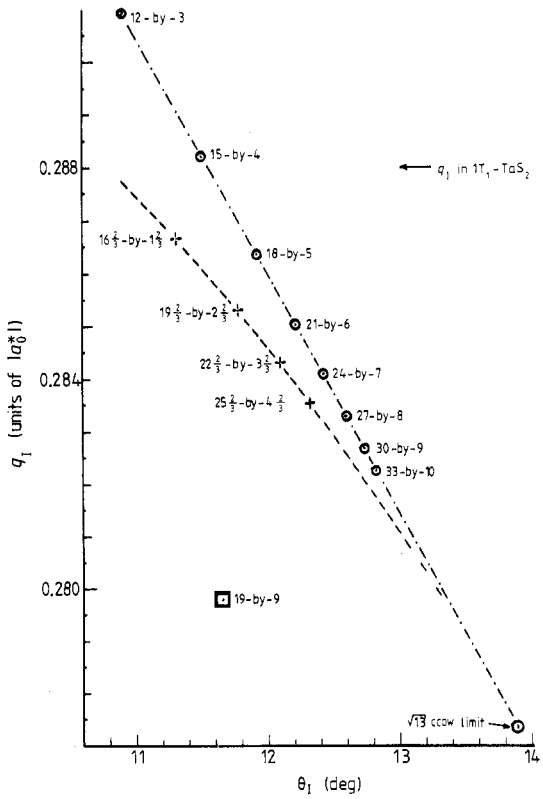

Figure 15. Possible staircase states in discommensurate families represented by 18-by-5 and $19\frac{2}{3}$-by-$2\frac{2}{3}$, stepping to $\sqrt{13}$ commensurate limit. Data for this figure can be found in table 3.

Table 3. Data plotted on figure 15.
(*a*) 18-by-5 family

a_D		Ta per domain	q_I	θ_I
9-by-2	10.149	103	0.2956	09°50′
12-by-3	13.748	189	0.2910	10°54′
15-by-4	17.349	301	0.2882	11°30′
18-by-5	20.952	439	0.2864	11°55′
21-by-6	24.556	603	0.2851	12°13′
24-by-7	28.160	793	0.2841	12°26′
27-by-8	31.765	1009	0.2833	12°36′
39-by-9	35.369	1251	0.2827	12°44′
3-by-1	3.606 in a_0	13	0.2773 in a_0^*	13°54′

(b) $19\frac{2}{3}$-by-$2\frac{2}{3}$ family

a_D		Ta per domain	q_I	θ_I
$16\frac{2}{3}$-by-$1\frac{2}{3}$	17.560	$308\frac{1}{3}$	0.2866	11°18′
$19\frac{2}{3}$-by-$2\frac{2}{3}$	21.126	$446\frac{1}{2}$	0.2853	11°46′
$22\frac{2}{3}$-by-$3\frac{2}{3}$	24.705	$610\frac{1}{3}$	0.2843	12°06′
$25\frac{2}{3}$-by-$4\frac{2}{3}$	28.290	$800\frac{1}{3}$	0.2835	12°20½′
	in a_0		in a_0^*	

θ_I to 0.05°), while by the latter it is difficult to eliminate creaking and mechanical 'give' in the imperfect crystals of layer compounds. We were encouraged to attempt the dilatometry by the work of Sezerman *et al* [22], whose paper presents contraction and expansion traces which seem to display several slight discontinuities. Clearly now the way to tackle the problem is by direct imaging at the atomistic level as a function of temperature using scanning tunnelling microscopy, and employing top quality material. Through direct monitoring of φ_D and a_D it should be possible to gauge whether the latter quantities (and therefore q_I and θ_I) slip continuously with temperature, or whether they jump discretely in a staircase sequence towards full $\sqrt{13}$ commensuration. Figure 15 shows the details of the possible states both in the $19\frac{2}{3}$-by-$2\frac{2}{3}$ family and also in the 18-by-5 family to which the former tends. The consistent emergence from the stripe phase at 273 K could well be triggered by such a step for the $1T_2$ phase. Staircase behaviour has yet to be reported for a true CDW, although there exist certain ferroelectric sequences, and among magnetic systems, where pinning by impurities is weaker, there are the remarkable spin orientation sequences examined recently in the rare earth metals Ho and Dy [23]. The invariance of q_I with respect to T in the ICDW states of $NbSe_3$ has always suggested to the author that those CDWs must show discommensurate order [24] and clearly STM work ought to be performed carefully now on $NbSe_3$ as a function of temperature, using good quality crystals vacuum-cleaved at low temperature to prevent selenium loss.

4. Conclusions

It has been possible from careful examination of electron diffraction data and scanning tunnelling microscopy images to solve the form of the structure of 'quasi-commensurate' $1T_2$-TaS_2. The strongly discommensurate structure is, despite first appearances, a true

half-way house between the $1T_1$ and $1T_3$ states. The structure actually adopted implies a significant stacking energy component in its selection. By performing the scanning tunnelling work as a function of temperature it ought to be possible to resolve whether the $1T_2$ state constitutes a unique intermediate state, or whether it is just the first step on a partial staircase of states, ultimately cut off by full lock-in at 180 K to the $1T_3$ state. Similar work should be performed on clean, high quality $NbSe_3$.

Acknowledgments

My thanks to D A Wilson for help in the production of this paper.

References

[1] Wu X-L and Lieber C M 1989 *Science* **243** 1703
[2] Wilson J A, DiSalvo F J and Mahajan S 1975 *Adv. Phys.* **24** 117
[3] (a) Brouwer R 1978 *PhD Thesis* University of Groningen
(b) Brouwer R and Jellinek F 1980 *Physica* B **99** 51
[4] (a) Hughes H P and Pollak R A 1976 *Phil. Mag.* **34** 1025
(b) Pollak R A, Eastman D E, Himpsel F J, Heimann P and Reihl D 1981 *Phys. Rev.* B **24** 7435
[5] (a) Pfeiffer L, Kovacs T and DiSalvo F J 1984 *Phys. Rev. Lett.* **52** 687
(b) Eibschutz M (Bell Laboratories) 1988 private communication
(c) Butz T, Vasquez A and Lerf A 1979 *J. Phys. C: Solid State Phys.* **12** 4509
[6] (a) Fung K K, McKernan S, Steeds J W and Wilson J A 1981 *J. Phys. C: Solid State Phys.* **14** 5417
(b) McKernan S, Steeds J W and Wilson J A 1982 *Phys. Scr.* T **1** 74
[7] Bird D M, McKernan S, Steeds J W and Withers R L 1985 *J. Phys. C: Solid State Phys.* **18** 481, 499, 519
[8] Wilson J A 1985 *J. Phys. F: Met. Phys.* **15** 591
[9] Fleming R M, Moncton D E, Axe J D and Brown G S 1984 *Phys. Rev.* B **30** 1877
[10] McMillan W L 1975 *Phys. Rev.* B **12** 1187, 1197; 1976 *Phys. Rev.* B **14** 1496; 1977 *Phys. Rev.* B **14** 643
[11] (a) Parsons J R 1976 *Proc. Microsc. Soc. Canada* **3** 22
(b) van Tendeloo G, van Landuyt J and Amelinckx S 1981 *Phys. Status Solidi* a **64** K105
(c) Iijima S and Bando Y 1981 *Proc. 39th Ann. Conf. EMSA* ed G W Bailey (Baton Rouge, LA: Claitors)
(d) Kuwabara M, Tomita M, Hashimoto H and Endoh H 1986 *Phys. Status Solidi* a **96** 39
(e) Withers R L and Steeds J W 1987 *J. Phys. C: Solid State Phys.* **20** 4019
[12] Withers R L and Wilson J A 1986 *J. Phys. C: Solid State Phys.* **20** 4809
[13] (a) Slough C G, McNairy W W, Coleman R V, Drake B and Hansma P K 1986 *Phys. Rev.* B **34** 994
See Coleman R V, Giambattista B, Hansma P K, Johnson A, McNairy W W and Slough C G 1988 *Adv. Phys.* **37** 559
(b) Thompson R E, Walter U, Ganz E, Clarke J, Zettl A, Rausch P and DiSalvo F J 1988 *Phys. Rev.* B **38** 10734
(c) Wu X-L, Zou P and Lieber C M 1988 *Phys. Rev. Lett.* **61** 2604
[14] Caldwell C W Jr 1974 *Bell Telephone Memo* **74** 1157–33
[15] Cantini P, Boato G and Collela R 1980 *Physica* B **99** 59
[16] Fleming R M, Moncton D E, McWhan D B and DiSalvo F J 1980 *Phys. Rev. Lett.* **45** 576
[17] (a) Tanda S, Sambongi T, Tani T and Tanaka S 1984 *J. Phys. Soc. Japan* **53** 476
(b) Tanda S and Sambongi T 1985 *Synth. Met.* **11** 85
(c) Withers R L and Steeds J W 1987 *J. Phys. C: Solid State Phys.* **20** 4019
[18] Wilson J A 1978 *Phys. Rev.* B **17** 3880
[19] Naito M and Tanaka S 1984 *J. Phys. Soc. Japan* **53** 1217
[20] Naito M, Nishihara H and Tanaka S 1984 *J. Phys. Soc. Japan* **53** 1610; 1986 *J. Phys. Soc. Japan* **55** 2410
[21] Herrenden Harker W G 1985 Postdoctoral *Thesis* University of Bristol; 1986 *Proc. Conf. Charge Density Waves (Budapest, 1985) (Springer Lecture Notes in Physics 217)* (Berlin: Springer) p76
[22] Sezerman O, Simpson A M and Jericho M H 1980 *Solid State Commun.* **36** 737
[23] Bates S, Patterson C, McIntyre G J, Palmer S M, Mayer A, Cowley R A and Melville R 1988 *J. Phys. C: Solid State Phys.* **21** 4113, 4125; and unpublished work
[24] Wilson J A 1982 *J. Phys. F: Met. Phys.* **21** 2469; 1985 *Phil. Trans. R. Soc.* A **314** 159–77